Synthesis of Conjugated Polymers Containing Terpyridine−Ruthenium Complexes: Photovoltaic Applications

Virginie Duprez,* Matteo Biancardo, Holger Spanggaard, and Frederik C. Krebs

The Danish Polymer Centre, RISØ National Laboratory, P.O. Box 49, DK-4000 Roskilde, Denmark

Received June 17, 2005; Revised Manuscript Received October 3, 2005

ABSTRACT: We report the synthesis of (*E*)-3-(4-bromo-2,5-dioctylphenyl)-2-(4-vinylphenyl)acrylonitrile (**5**). We further report the synthesis of conjugated polymer materials by palladium-catalyzed Heck coupling polymerization of **5** and 4-bromo-2,5-dioctyl-4′-vinylstilbene (**3**) in the presence of 4′-(4-bromophenyl)-2,2′:6′,2″-terpyridine (**8**), giving poly(dioctylstilbenevinylene)s terminated by a terpyridine moiety. Their assembly using ruthenium complexation led to coordination homopolymers and copolymer with tetrafluoroborate counterions. The materials were characterized using SEC, MALDI, NMR, UV−vis, and fluorescence spectroscopy. The polymers were found to transfer energy to the complexes as seen through the complexes ability to quench fluorescence. The coordination polymers were applied to photovoltaics, and two types of devices were prepared: polymer solar cells obtained by spin-coating of the coordination polymer solution onto PEDOT:PSS-covered ITO substrates and dye-sensitized solar cells obtained by absorption on TiO_2 nanocrystalline films using two different electrolytes. Dye-sensitized solar cells (DSSCs) prepared using the copolymer **15** gave the best results with efficiencies reaching ∼0.1% with the redox couple $Co^{II,III}$ as electrolyte, whereas the coordination homopolymer **13** gave the best results as organic solar cells with very low efficiency (<0.01%) under illumination at 1000 W/m^2 AM1.5.

Introduction

Semiconducting polymers such as substituted poly(*p*-phenylenevinylene)s (PPV's) have become well-known for their properties in the context of polymer electronic devices. Recently, their complexation with transition metals have been investigated, and a number of publications presenting the studies of PPV's,[1] thiophenes,[2] or others polymers[3] coordinated with ruthenium have been published.

The incorporation of a ruthenium complex into a conjugated polymer has the potential to facilitate the charge carrier generation. Such metal complexes usually exhibit a reversible $Ru^{II,III}$ redox process and some ligand-centered redox processes. In addition, a metal complex incorporated into a polymer will influence the optical and electronic properties of the polymer due to its characteristic metal-to-ligand charge transfer (MLCT) transition around 500−600 nm, thus extending the absorption range of the material. Among the transition metal complexes, one of the most commonly used and studied is the chromophore ruthenium(II)−bis(terpyridyl), $Ru(tpy)_2$, which is a well-known photoactive spacer.[4]

Terpyridine ligands are effective complexing agents and key building blocks[5] in supramolecular chemistry, and their 4′-substitution is also particularly attractive because it leads to the construction of linear, rodlike polynuclear polymers and complexes. There are several different possibilities to link these functional components, and finding the right synthetic route is the most challenging part. Our approach was to carry out the polymerization of the respective monomers in the presence of the terpyridine ligand followed by complexation with ruthenium and further ligand exchange reaction with the second polymer block. The polymer blocks that we prepared were PPV's of the OF[6] and CNOF[7] type, different from each other by the presence of a cyano substituent on the vinylene group and thus leading to two types of terpyridine−polymer blocks: one with a donor character called OF and one with an acceptor character called CNOF (Scheme 1). Indeed, Heeger and co-workers[8] have shown that the blending of donor (MEH−PPV) and acceptor (CN−PPV) polymers with different $\pi-\pi^*$ energy gaps can optimize the photoinduced charge separation. Our motivation for synthesizing such supramolecular architectures is to show that the difference in electronic character provided by the greater electron affinity of the CNOF combined with the lower ionization potential of the OF[9] (Table 1 and Figure 1) compared to the CNOF[7] is sufficient to provide a photoinduced charge separation enhanced by the energy transfer from the polymer to the ruthenium complex.

The study of the coordination polymer consisting in the PPV donor (OF) and the PPV acceptor (CNOF) separated by the photoactive spacer $Ru(tpy)_2$ is of particular photovoltaic interest, and its comparison with the architectures prepared only from the PPV donor

Scheme 1

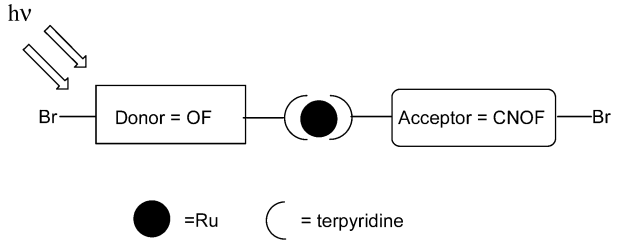

Table 1. Data from the Photoelectron Spectra for Thin Films of the Polymers OF and CNOF on Gold Substrates

compound	E_F^{VB}	E_F^{VAC}	Δ	IP	E_{gap}(UV−vis)
OF[a]	0.7	4.7	−0.2	5.4	2.58
CNOF[b]	1.4	4.3	−0.4	5.7	2.54

[a] Values were taken from ref 9 and corrected according to the reference: Krebs, F. C.; Jørgensen, M. *Macromolecules* **2004**, *37*, 3958. [b] Data taken from ref 7.

* Corresponding author: e-mail virginie.duprez@risoe.dk.

10.1021/ma051274f CCC: $30.25
Published on Web 11/10/2005

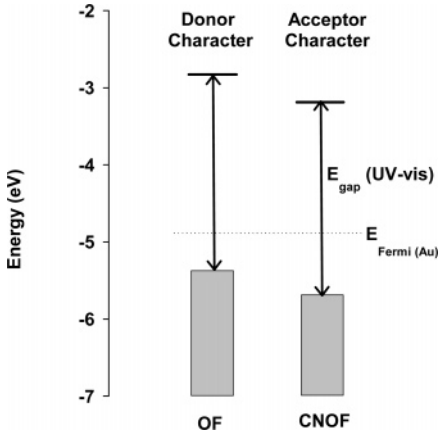

Figure 1. Representation of the energy levels as observed on thin films of the polymers on a gold substrate using ultraviolet photoelectron spectroscopy. The filled boxes indicate the filled levels, and the E_g is the band gap determined using the UV−vis spectra.

(OF) type or from the PPV acceptor (CNOF) is of comparative interest. The synthesized conducting polymer blocks have different electronic energy levels to provide one path for the electrons and one path for the holes. The light harvesting of the polymer blocks and the energy transfer to the ruthenium complex were contemplated to allow for carrier generation by exciton dissociation.

Such an assembly present several features such as (i) studying the influence of the presence of a cyano group leading to an electron-deficient polymer block considered as our acceptor moiety that should increase electronic conduction compared to the polymer block without cyano substituent, which is the donor moiety; (ii) understanding the role of the ruthenium complex incorporated in a PPV type polymer in terms of energy transfer via photophysical studies and photovoltaic applications; and (iii) applying these new materials in solar cells using different approaches to enhance the efficiency of the resulting cells.

These approaches can be the preparation of different types of device such as polymer solar cells and dye-sensitized solar cells. Another alternative is to combine a ruthenium polymer with a zinc porphyrin species to obtain a charge-separated state with a long lifetime[4b] through the electron transfer between the porphyrin and the ruthenium polymer. The photophysical and photovoltaic studies of the thin films will provide information about the mechanism of energy transfer between these assemblies when they are not covalently linked. Since the synthetic procedure leading to the assembly of a coordination polymer with a zinc porphyrin is very challenging, such a device will be of big interest in the case of enhancement of the efficiency.

In this paper, we present the synthetic pathway developed for the preparation of the polymer blocks containing terpyridine moieties and their combination via ruthenium complexation leading to the ruthenium homopolymer and copolymer. The spectroscopic characterization and photophysical properties of the different compounds will be discussed. The coordination polymer compounds have been applied for photovoltaics and discussed using different strategies.

Results and Discussion

Synthesis of Polymers and Polymer−Metal Complexes. The synthetic paths leading to monomer units differing only from each other by the presence of a cyano substituent on the vinylene part are shown in Scheme 2. One of the synthetic routes involves the Horner−Wadsworth−Emmons reaction between the known starting materials 1-bromo-4-formyl-2,5-dioctylbenzene[10] (**1**) and diethyl 4-phosphonatomethylstyrene[11] (**2**). 4-Bromo-2,5-dioctyl-4′-vinylstilbene[12] (**3**) was obtained in 33% yield. A Knoevenagel type condensation between 1-bromo-4-formyl-2,5-dioctylbenzene[10] (**1**) and vinylacetonitrile[13] (**4**) led to the cyanovinylene analogue (*E*)-3-(4-bromo-2,5-dioctylphenyl)-2-(4-vinylphenyl)acrylonitrile (**5**) with a yield of 45%.

The raw compounds **3** and **5** were respectively reprecipitated from hexane and absolute ethanol using a CO_2(s)/acetone bath until complete removal of small amounts of unreacted starting materials or condensation products. This gave the pure monomers **3** and **5**. These compounds could be kept for long periods of time under argon in the freezer without degradation.

The polymers **6** and **7** were obtained using the palladium-catalyzed Heck coupling reaction with $Pd_2(dba)_3$/tri-*tert*-butylphosphine tetrafluoroborate as a catalytic system and *N*-methyldicyclohexylamine as a base[12] in order to achieve a directional synthesis. The compounds **6**[10,12] and **7**[7] were purified using *N*,*N*-diethylphenylazothioformamide[14] since we recently demonstrated that the incorporation of palladium nanoparticles[15,16] during the Heck reaction degraded the properties of thin films prepared from these polymers.

Using monomers substituted at one end with a halogen and a vinyl group at the other end is very suited for the incorporation of a terpyridine substituted in the 4′-position with a bromophenyl at the end of the polymer backbone.

It was possible to synthesize the PPV−terpyridine **9** and **10** as shown in Scheme 3 through palladium-catalyzed polymerization using the same catalytic system as previously in the presence of 4′-(4-bromophenyl)-2,2′:6′,2″-terpyridine.[17] Attempts performed with a molar ratio of 1:1 between the terpyridine and the monomer were unsuccessful for the incorporation of terpyridine in the polymer and led only to polymers **6**, **7**, and unidentified compounds. However, a molar ratio of 1:2 between the terpyridine and the monomer was proven to give an average chain length of up to 8 monomer units (see Supporting Information Table S1).

The monomers **3** and **5** were converted into a mixture of polymers. The compounds were purified by a preliminary column chromatography in order to remove the polymers without terpyridine moieties that do not bind strongly to silica in chloroform from the ones containing terpyridine that bind strongly to silica in chloroform but that can be eluted using THF. A second purification step using a dry column vacuum chromatography[18] was required, using an eluent consisting of 0−5% ethyl acetate in 1,2-dichloroethane. Since the reaction also gives oligomers with low molecular weight like monomer−tpy, dimer−tpy, and unidentified byproducts, the desired compounds **9** and **10** were obtained in low yield. The removal of the byproducts and lower oligomers was found to be essential in order to obtain polymer−tpy with a chain length of a few monomer units. A recent study[19] has shown that the monomer has an extinction coefficient around 55 000 M^{-1} cm^{-1}, the dimer around $\epsilon_{\lambda_{max}} = 84\,000$ M^{-1} cm^{-1}, and the trimer, tetramer, and pentamer around $\epsilon_{\lambda_{max}} = 135\,000$ M^{-1} cm^{-1}. The selective preparation of the PPV−tpy ligands with a specific

Scheme 2. Synthetic Route Leading to the Monomer Units and the PPV's Type Polymers

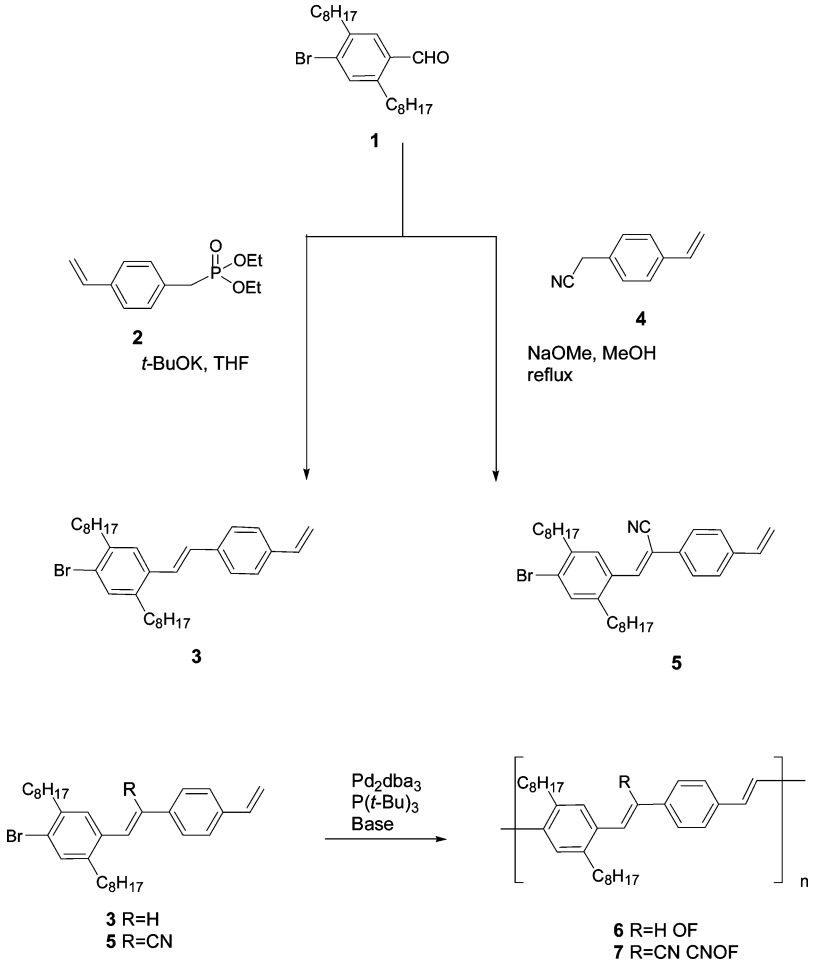

number of monomer units through a palladium-catalyzed polymerization cannot be controlled from a synthetic point of view. However, this purification in two steps was proven to lead to a mixture of PPV−tpy having very similar optical properties. Another way to obtain very selectively a trimer, tetramer, or pentamer−tpy would consist in carrying out a stepwise and directional synthesis,[19] but this synthetic pathway has not been successful for the monomer having a cyano group.[7]

The number of units in the polymer was determined by using NMR and size exclusion chromatography (SEC), and the incorporation of terpyridine in the polymers was proven by using the NMR and the MALDI−TOF. The polymers were characterized by NMR, SEC, MALDI−TOF MS, and UV−vis spectroscopy.

The fractions containing more than two monomer units were used to prepare the coordination polymers. Some problems of solubility were encountered with the polymers synthesized. Compounds **6**, **7**, **9**, and **10** were found to be only partially soluble in chloroform. However, after reaction with ruthenium, the ionic complexes were highly soluble in chloroform.

The coordination homopolymers were prepared according to Scheme 3. In a typical complexation of the polymers−tpy **9** and **10**, an appropriate quantity of $RuCl_3 \cdot 3H_2O$ was reacted with 2 equiv of **9** or **10** in a mixture of DMF/ethanol under reflux at 110 °C. The first water ligand exchange with 1 equiv of polymer−tpy proceeds easily; however, the chloride exchange is more difficult to achieve and requires activation. The monosubstituted trichloride complex was then activated using the system $AgBF_4$/acetone whereby the chloride is exchanged for acetone. The ruthenium(III) was reduced to ruthenium(II) by the presence of ethanol which acts as a reducing agent to give the coordination polymers **12** and **13**. The products were precipitated as dark red fibrous solids after concentration of the reaction volume under vacuum and addition of water.

The coordination copolymer **15** was prepared according to the same method used for the ruthenium polymers **12** and **13** with the following differences. The $RuCl_3 \cdot 3H_2O$ was first reacted with 1 equiv of **10** in a mixture of DMF/ethanol under reflux. The resulting coordination Ru(III) complex was activated with 3 equiv of $AgBF_4$/acetone under reflux for 2 h. A solution of **9** in DMF was then added to the reaction mixture, and the solution was heated under reflux overnight.

The coordination polymers **12**, **13**, and **15** were characterized by their ^1H NMR spectra, their UV absorption, and emission spectra.

MALDI−TOF was also used in order to confirm that there was no ruthenium chloride species present in the reaction mixture and to detect characteristic peaks in the range of the expected molecular weight. The MALDI−TOF mass spectra were very complex to interpret due to the fact that the polymer−tpy employed for the synthesis of the complexes was already a mixture of molecules with different chain length. As a result, a combination of all the different polymers present in the starting polymer−tpy coordinated via ruthenium was

Scheme 3. Synthetic Pathway Leading to the Complexes 12, 13, 15, and 16

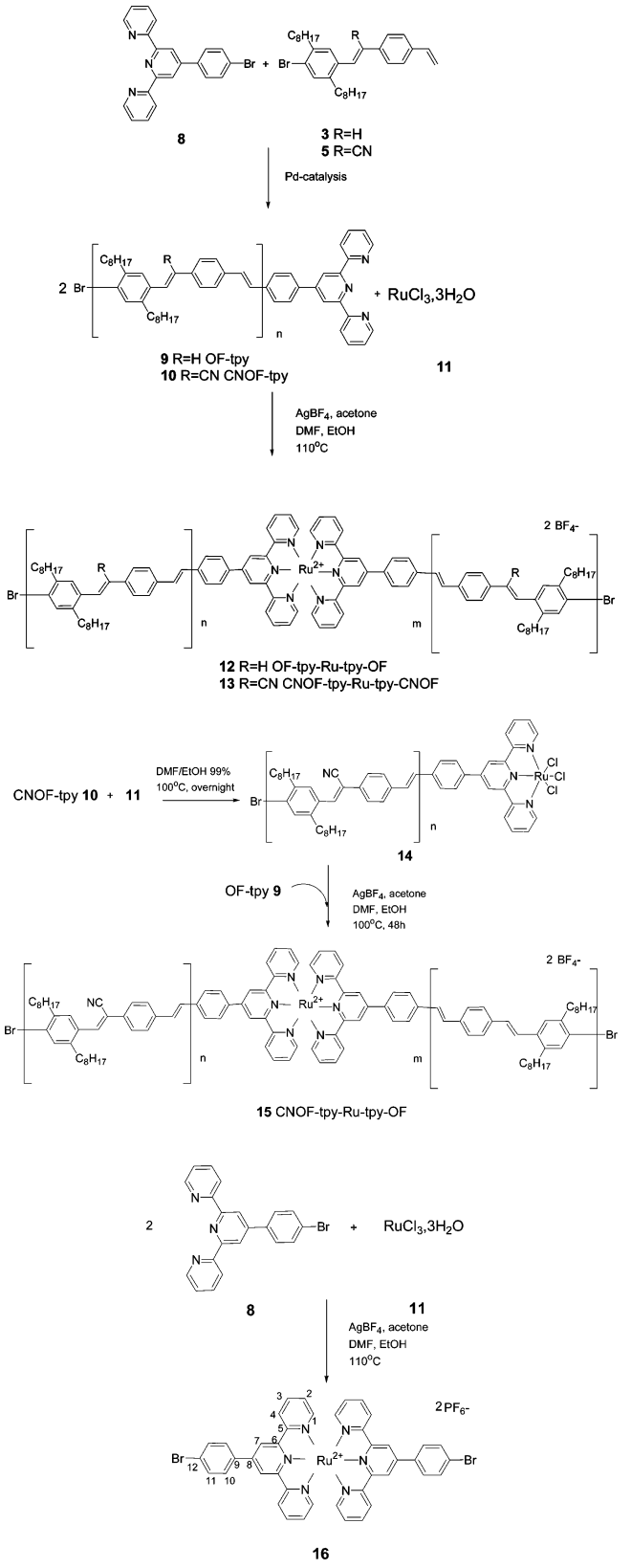

obtained, leading to a large number of peaks differing by only one monomer unit. Some additional peaks due to fragmentation were also observed.

Structural Characterization. NMR Spectra. Figure 2 shows the respective ^{1}H spectra of **5**, **8**, and **10** agree with the polymeric nature of the CNOF−terpyridine **10** as well as the incorporation of the terpyridine in the polymer during the polymerization reaction. The spectrum of monomer **5** (middle) shows the signature of the vinyl end protons at 6.74, 5.84, and 5.35 ppm. The peaks at δ = 7.47−7.76 ppm are due to the phenylene−vinylene units. The peaks at δ = 2.79−2.58, 1.67−1.25, and 0.84 ppm are attributed to the octyl side chain. In the spectrum of **10** (top), the signals corresponding to the vinyl end groups are no longer present, and the integration of the alkyl chains and the phenylene−vinylene units confirms the presence of the polymer. In addition, the spectrum of **10** displays new signals at low field between 8.79 and 8.69 ppm, characteristic of the terpyridine signature. The spectrum of **8** (bottom) shows the assignment of the terpyridine protons in order to attribute the patterns corresponding to the terpyridine unit in the spectrum of **10**.

Table 2. Molecular Weights of Different Fractions of the PPV−Terpyridine Used for the Preparation of the Coordination Polymers

compound/fraction[a]	**9**/5	**9**/6	**10**/4	**10**/5
mol wt	2750	1785	3446	2372
complex[b]	**15**	**12**	**15**	**13**

[a] These fractions were isolated after the dry column vacuum chromatography. The previous fractions eluted were not reported because of their very low concentration. [b] Each of these fractions was used to synthesize a specific complex.

The molecular weight of the polymer−tpy was determined using the ^{1}H NMR spectroscopy. The monomer **5** has two octyl substituents; thus, six protons for the two terminal methyl groups on the alkyl chains and the terpyridine has a multiplet in the aromatic area (8.65−8.74 ppm) corresponding to six protons.[17] The ratio between the integration corresponding to the methyl groups and the average number of the protons of the terpyridine/monomer gives information on the average length of the polymer chain. The details of the determination of the molecular weight of one of the representative fractions of the CNOF−terpyridine **10** are given below.

The molecular weight of the different fractions of CNOF/OF−terpyridine **9** and **10** was calculated as follows considering the data of the ^{1}H NMR spectra (Figure 2).

$$\text{molecular weight} = ((26.18/6) \times 454.71) + 308.36 + 79.904 = 2372 \text{ g mol}^{-1}$$

26.18 corresponds to the integration of the CH_3 of the alkyl chain, 454.7 is the molecular weight of the monomer **6** without the bromine, 308.36 is the molecular weight of the terpyridine without the bromine, and 79.9 corresponds to a bromine atom. Table 2 summarizes molecular weights of different PPV−terpyridine fractions. These fractions were used for the synthesis of the coordination polymers.

To assign the different signals of the terpyridine moieties after coordination with a metal complex, the model complex bis[4′-(4-bromophenyl)-2,2′:6′,2″-terpyridine]$^{2+}$−ruthenium(II) (**16**) was prepared according to known procedures[4a,b,17b] from the literature and compared with the NMR of **15** recorded in a 1:1 mixture of $CDCl_3$/ DMSO-d_6. As shown in Figure 3, the signals of the protons H_7, H_4, and H_3 of the terpyridine in **15** are in the same range of those obtained for the model complex **16** (see assignment Scheme 3). The signals display a much broader pattern in **15** due to the polymeric nature of the terpyridine ligand. The other

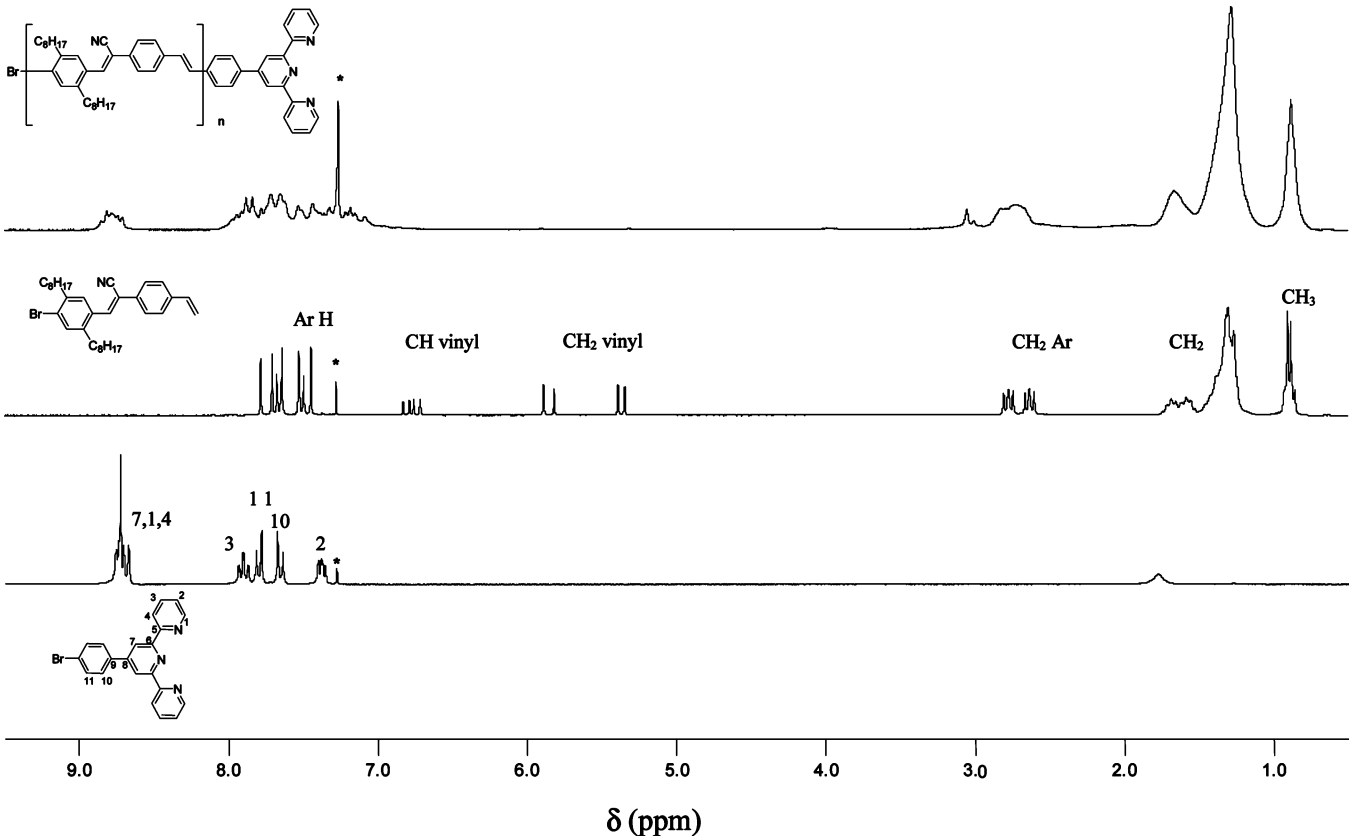

Figure 2. ^{1}H NMR spectra of 4′-(4-bromophenyl)-2,2′:6′,2″-terpyridine (**8**) (bottom), (*E*)-3-(4-bromo-2,5-dioctylphenyl)-2-(4-vinylphenyl)acrylonitrile (**5**) (middle), and the CNOF−terpyridine (**10**) (top) recorded in $CDCl_3$ at room temperature. The deuterated solvent is marked with an asterisk.

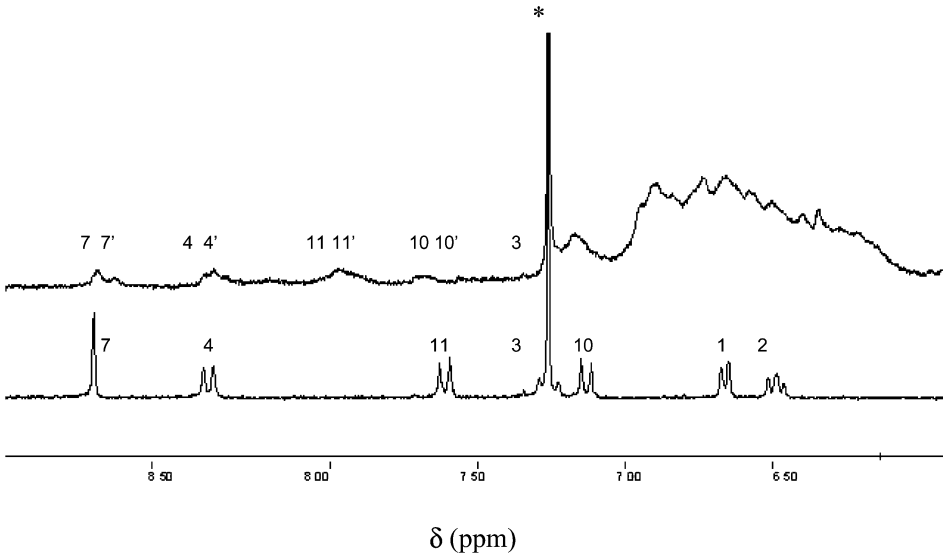

Figure 3. The aromatic region of the ^{1}H NMR spectra for the terpyridine signals in the model complex **16** (bottom) and ruthenium copolymer **15** (top) recorded in DMSO-d_6/$CDCl_3$ at room temperature. The deuterated solvent is marked with an asterisk.

significant difference is the appearance of broad signals to chemical shifts equal to 8 and 7.5 ppm due to the proton resonance of H_{10} and H_{11} on the phenyl substituent in the 4′-position on the terpyridine. Indeed, the terpyridine is connected to a vinyl group in **15** instead of a bromine in the model complex **16**.

In addition, a solvatation effect due to the nature of the deuterated solvent used was observed and a less resolved pattern was obtained for **15** in $CDCl_3$ (see Figure S1 in Supporting Information). Only broad signals were observed at room temperature due to the polymeric nature of the complex, and the expected terpyridine signals were not clearly visible due to their rather low concentration in the polymer.

After analysis of the ^{1}H NMR spectra, the integration of the pattern relative to the polymer part vs the ruthenium complex pattern showed that the molecular weight obtained from the spectra was lower than expected. This can be due to the fact that not all the PPV−terpyridine present in the fraction used to synthesize the coordination polymers was complexed with ruthenium during the reaction.

Table 3. Molecular Weights of Some Representative Polymers As Determined by SEC Using a Polystyrene Standard Series

compound	**6**[b]	**7**[b]	**9**/5[c]	**9**/6[c]	**10**/4[c]	**10**/5[c]
M_n/PD	4515/2.58	3675/1.77	-[d]	1628/1.18	3760/2.06	2767/1.51
M_{peak}[a]	3204	3793	-[d]	1904	3427	2508
λ_{max} (nm)	400	400	403	405	406	405

[a] The molecular peak was obtained through the SEC. [b] The molecular weights of the polymers **6** and **7** were determined by SEC with a fixed wavelength of 400 nm. [c] The notations **9**/5, **9**/6, **10**/4, and **10**/5 correspond to the fraction numbers of the respective compounds **9** and **10**. The previous fractions were not reported because they were not used for the preparation of the coordination polymers. [d] The SEC analysis was not performed due to the insufficient amount of the sample.

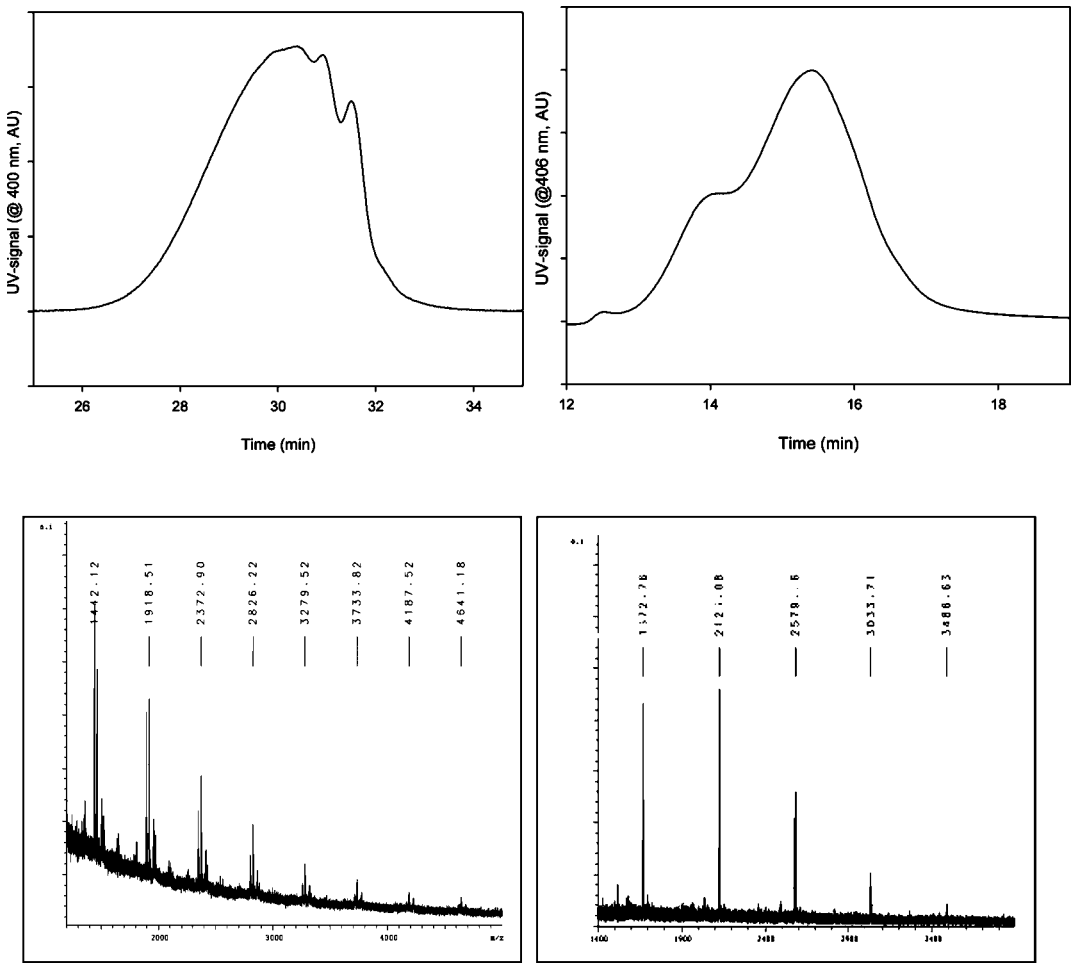

Figure 4. SEC characterization of the polymer **7** (top left) using a column with pore volumes of 500, 10 000, and 1 000 000 Å and of one of the representative fractions of CNOF−tpy **10/4** (top right) using a column with pore volumes of 100 and 1000 Å. MALDI−TOF mass spectrum of polymer **7** using dihydroxybenzoic acid (DHB) as a matrix (bottom left). MALDI−TOF mass spectrum of **10/4** which is a mixture of higher oligomers (bottom right).

Size Exclusion Chromatography and MALDI−TOF. In addition to NMR characterization, the molecular weights of the polymer were determined using size exclusion chromatography (SEC) with UV−vis detection and MALDI−TOF.

According to the results summarized in Table 3, the values of the M_{peak} are in agreement with the molecular weight calculated using the ^{1}H NMR spectra (see Table 2). These values display an important difference of molecular weight and chain length between the different fractions of compounds **9** and **10**. This difference could influence the properties of the resulting coordination polymers in their photovoltaic application.

As seen in Figure 4, the chromatogram of the polymer **7** presents a broad dispersion of molecular weights. Individual oligomers are visible in the low molecular weight range. However, the chromatogram of **10**/4 displays a mixture of three major compounds, assigned to be trimer, tetramer, and pentamer with small amount of hexamer and heptamer according to the results obtained from the MALDI−TOF (Figure 4). This fraction was not further purified and was used for the preparation of the ruthenium complexes.

Several attempts to determine the molecular weights of the coordination polymers containing tetrafluoroborate counterions using SEC failed. Despite reported success[1b] in obtaining SEC data for ionic Ru complexes, we were not able to obtain pure size exclusion with ionic species due probably to interaction with the column material. We believe that the complexes are stationary in the SEC column due to their ionic nature, and we currently have no solution to this problem.

UV−vis. The electronic absorption spectra recorded in chloroform solution are summarized in Table 4. The

Table 4. UV−vis Data for Monomers, Polymers, and Ruthenium Coordination Polymers Recorded in Chloroform Solution and Thin Film

compounds	$\lambda_{max\ sol}$ (nm) ($10^3\epsilon$ ($M^{-1}\,cm^{-1}$))	$\lambda_{max\ film}$ (nm)
3	328 (36.6)	
6	418 (37.7)	
5	334 (26.1)	
7	413 (36.3)	
9[a]	284 (35.1), 348 (27.9)	
10[a]	284 (12.2), 397 (3.4)	
12[b]	502, 367, 334, 313	506, 378
13[b]	493, 401, 333, 313	504, 416
15[b]	496, 398, 315	506, 400
16[c]	285 (58.9), 310 (58.7), 489 (24.6)	

[a] Determination of ϵ was calculated considering the molecular weight determined using the ^{1}H NMR spectra. [b] Determination of ϵ could not be determined reliably thus only the position of the maxima is reported. [c] The spectrum of the model complex **16** was recorded in acetonitrile.

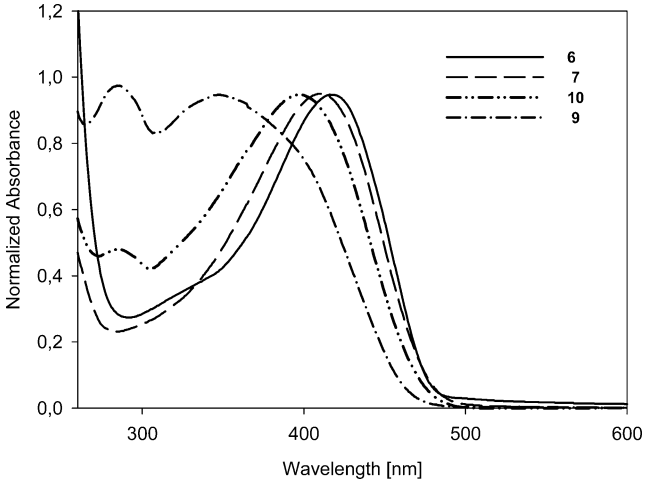

Figure 5. UV−vis absorption of the polymers (**6, 7**) and the terpyridine polymers (**9, 10**). The spectra are normalized according to λ_{max} of the polymer.

only difference in electronic properties between compounds **3**, **6** and **5**, **7** is due to the presence of the cyano[7,20] substituent in **5** and **7**.

Table 4 displays the absorption peaks of the monomers **3** and **5** and the polymers synthesized with and without incorporation of terpyridine. The absorption of **5** is red-shifted compared to **3** despite the cyano substituent entering into conjugation with the styrene backbone, increasing the π-electron delocalization. A bathochromic shift is observed between monomeric (~330 nm) and simple polymeric species (~410 nm) due to conjugation. In **7**, the absorption is blue-shifted compared to **6** (Figure 5) due to the presence of the high field ligand CN in compound **7**. This behavior should be the same for the polymers containing a terpyridine moiety and **10** should be blue-shifted compared to **9**. However, the opposite phenomenon is observed and **9** is blue-shifted. In this case, the higher molecular weight of **10** overtake the effect of the CN ligand. Lower extinction coefficients were obtained for the compounds containing cyano groups due to the steric effect of the cyano groups[20c,d] (see Table 4). After incorporation of terpyridine moieties in the polymeric ligand, an overlap of two main absorption bands (Figure 5) is observed. One sharp band (~280 nm) corresponds to the presence of the terpyridine, and the broad band in the visible (360−400 nm) is due to the polymer.

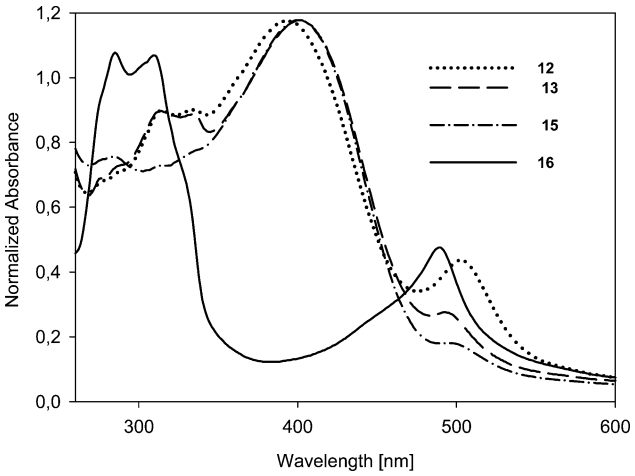

Figure 6. UV−vis absorption of the model complex **16**, the coordination homopolymer complexes **12** and **13**, and the coordination copolymer **15**.

Figure 6 displays the absorption spectra of a series of ruthenium(II) complexes described above to analyze the absorption behavior of the $[Ru(tpy)_2]^{2+}$ as a function of the substitution pattern of the ligands. In all the spectra of the ruthenium coordination polymers, intense absorption bands are observed at wavelengths below λ = 400 nm, which can be assigned to polymer centered $\pi \rightarrow \pi^*$ transitions (around 390−400 nm) and a broad less intense one (290−330 nm) which can be assigned to $\pi \rightarrow \pi^*$ transitions in the pyridine moieties.

The metal-to-ligand charge transfer (MLCT) is in the range of 493−502 nm in the 3 coordination polymers, and a slight bathochromic effect is observed due to the presence of cyano susbtituents on the polymeric ligand. The cyano group is a high field ligand that lowers the highest occupied molecular orbital (HOMO) of the molecule, leading to an increase of the Δ_0 (difference between the energy levels) and thus to a shift of the MLCT absorption to lower wavelengths by ~10 nm. This difference in the optical absorption properties gives significant information to characterize the different coordination polymers. The MLCT absorption band of the copolymer **15** is at 496 nm between the two homopolymers, slightly shifted to lower wavelength due to the presence of cyano groups in one of the two polymer blocks. A shift ~20 nm of the polymer absorptions was observed as a function of the length of the species under consideration. The length of the species does not have any influence on the MLCT and affects the $\pi \rightarrow \pi^*$ transitions (see Supporting Information Figures S2 and S3). By comparison with the spectrum of the model ruthenium complex **16** recorded in acetonitrile due to insolubility in chloroform, no significant shift of these absorptions was observed as a function of the length of the ligands. A slight bathochromic effect can be attributed to the solvent effect. The absorption spectrum of the complex **16** agrees with the incorporation of the $Ru(tpy)_2$ complex into the polymers synthesized. UV−vis spectra of thin films spin-coated onto glass slides from chloroform solution has shown a red shift of the absorption maxima in the films compared to the absorption maximum obtained for the coordination polymers in solution (see Table 4).

Luminescence Properties. The emission spectra of the terpyridine−PPVs **9** and **10** and the complexes **12, 13, 15**, and **16** are shown in Figure 7. The emission of **9** and **12** peaks around 480 nm, whereas the emission

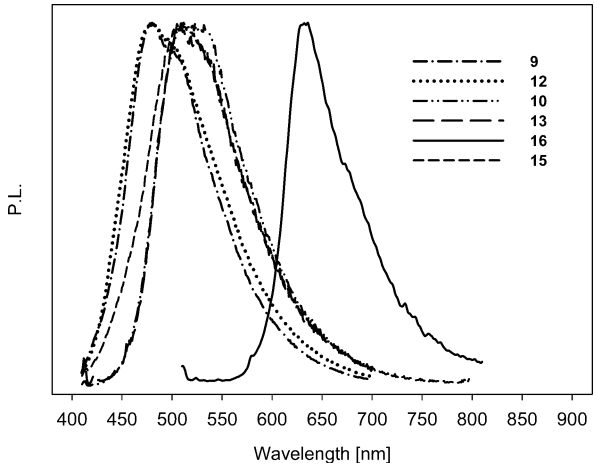

Figure 7. Normalized emission spectra of the terpyridine-PPVs **9** and **10** and the complexes **12**, **13**, **15**, and **16**, all recorded in degassed chloroform at RT. The compounds **9**, **10**, **12**, **13**, and **15** are excited at 400 nm, whereas **16** is excited at 490 nm.

Table 5. Emission Properties of the Terpyridine−PPV Derivatives and Their Coordination Polymers[a]

compound	emission peak (nm)	QY (%)	lifetime
9	480	63	~1 ns
10	480	7.6	
12	510	15	<100 ps
13	510	1.6	
15	510	7.0	
16	630	0.2	

[a] All measured in degassed chloroform at RT. Quantum yield are measured using 9,10-diphenylanthracene (DPA) as reference.[21]

of **10**, **13**, and **15** peaks around 510 nm. Emission of the model compound **16** peaks around 630 nm. The emission of **12** and **13** is very similar to the emission of **9** and **10**, and there is no sign of emission from the Ru complex. However, the quantum yield (QY) of the complexes **12** and **13** decreases by a factor of 4−5 compared to the polymers **9** and **10**. This could indicate that a substantial part of the excitons formed on the polymer are transferred to the complex. The terpyridine−Ru complex emits around 650 nm and has a QY below 0.02% according to the literature.[4b] (We measured the QY of the bromo derivative **16** and found a quantum yield of 0.2%.) Therefore, energy transfer to the complex will efficiently quench luminescence. The quantum yields and emission peaks are shown in Table 5.

To further establish that energy transfer indeed takes place, luminescence studies were conducted at 77 K in a 5:5:2 solvent mixture of diethyl ether:2-methylbutane: ethanol of the three complexes **12**, **13**, and **15**. As the temperature decreased, the polymer emission became narrower and emission in the 650−680 nm range increased, indicative of increased emission from the terpyridine−Ru complex moiety (see Figure 8). The complex emission is most clear in the case of **12**. This indicates that intramolecular energy transfer takes place. Since the Ru complex absorbs around 500 nm, where the polymer emits, the energy transfer may be of the Förster[22] type. If the QY decrease is due to energy transfer to the less luminescent Ru complex, around 80% of the excitons formed on the polymer may be transferred to the complex.

In the solid state the complex emission becomes much more dominant than the polymer emission. This is shown in Figure 9. We ascribe the more efficient energy

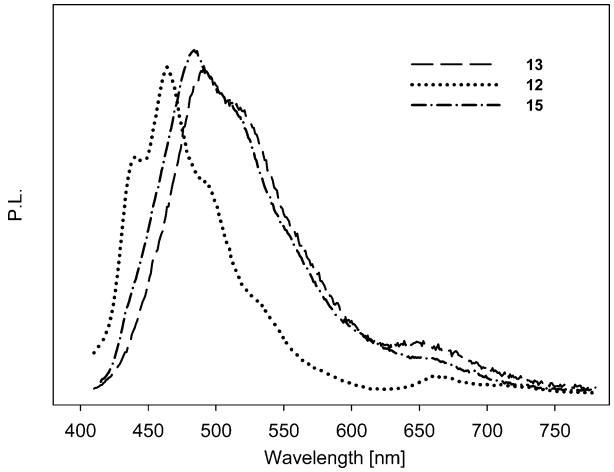

Figure 8. Normalized emission spectra of **12**, **13**, and **15** recorded in a 5:5:2 solvent mixture of diethyl ether:2-methylbutane:ethanol degassed at 77 K. Notice the emission of the terpyridine−Ru complex moiety above 630 nm. Excitation wavelength is 400 nm.

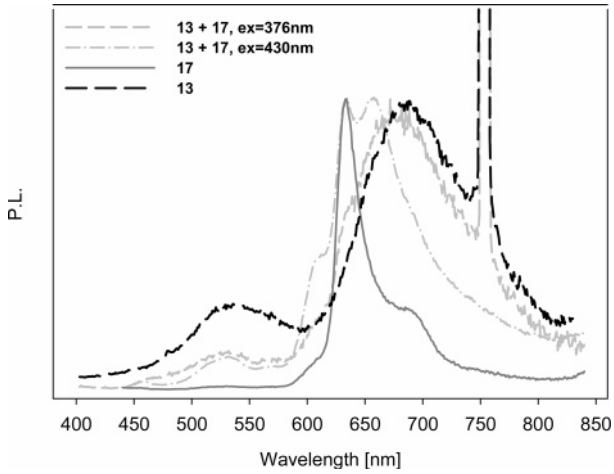

Figure 9. Normalized emission spectra of spin-coated films of **13** and **17** and blends of the two at RT. The sharp peaks at 752 nm is due to second-order diffraction from the excitation monochromator.

transfer to intermolecular energy transfer from the polymer to the complex moiety induced by shorter intermolecular distance in the solid state.

To study the mechanism of energy transfer between a coordination polymer and a zinc porphyrin when the two architectures are not covalently connected, we have combined them by simple mixture to process thin solid films and study their photophysical and photovoltaic properties. Two zinc porphyrins, the tetraphenyl-21*H*,-23*H*-porphyrin zinc (**17**) and the zinc-porphyrin-linked oligothiophene[23] (**18**), were employed to process the films (Scheme 4). For reasons of simplicity, only the blending effect of **17** was discussed since the porphyrin **18** has oligothiophene substituents which emit at the same wavelength 550 nm as CNOF−tpy **10**.

The effect of blending **17** with **13** in the solid state was investigated. Films were spin-coated from chloroform using 10 equiv of **17** w/w. Spectra of the blend and spin-coated **17** film are shown in Figure 9. Exciting the blend at 430 nm, where the porphyrin[24] has a very strong absorption, shows emission from both the Ru complex and the porphyrin. There is also a weak polymer emission around 525 nm, which is probably due to the fact that the polymer also absorbs at 430 nm,

Scheme 4

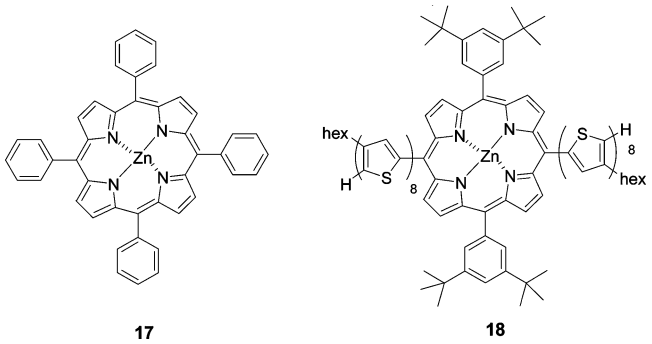

17 **18**

Table 6. Summary of the Photovoltaic Performance of Polymer Solar Cells Based on the Compounds Synthesized Using the Same Device Geometry (1000 W m^{-2}, AM1.5)

device geometry	I_{sc} (μA/cm^2)	V_{oc} (mV)	R_{dark} (Ω)[a]
ITO/PEDOT:PSS /**12**/Al	1.1	3	460
ITO/PEDOT:PSS/**12**/C_{60}/Al	9.2	62	85000
ITO/PEDOT:PSS /**13**/Al	10.6	315	23000
ITO/PEDOT:PSS /**15**/Al	5.0	78	15000
ITO/PEDOT:PSS /**18**/Al	7.6	175	1600
ITO/PEDOT:PSS/**13:18**/Al	2.4	425	95000
ITO/PEDOT:PSS/**12:17**/Al	5.7	16	800
ITO/PEDOT:PSS/**13:17**/Al	5.8	16	470

[a] The value for R_{dark} depends on the device geometry with an active area of ~3 cm^2. The positive terminal was connected to the transparent ITO electrode, and the negative terminal was connected to the metal electrode.[19]

albeit much weaker than the porphyrin. It can be seen that some energy transfer from the porphyrin to the Ru complex takes place. However, the energy transfer is only partial, which could be due to a less perfect blend in the solid state. Thus, some porphyrins may not have a Ru complex in the vicinity. When the blend is excited at 376 nm, where the polymer absorbs more intensely than the porphyrin, the porphyrin emission decreases dramatically in the solid state. It thus seems that when the blend is excited, energy tends to find a path to a Ru complex rather than to the porphyrin. However, it should be remembered that these photophysical measurements do not reveal details of the nonluminescent energy. It could be that a substantial fraction of energy harvested by the blend actually may end on the porphyrin moiety but is lost by a nonradiative path.

Photovoltaic Cell Characterization. Photovoltaic cells based on coordination polymers synthesized above were assembled using two types of devices: polymer solar cells and dye-sensitized solar cells (see Supporting Information Figures S4 and S5).

All Polymer PV Devices. The results collected have been summarized in Table 6. The efficiencies were very low (<0.01%), and the results in Table 6 are meant to illustrate the differences between the compounds used in the same device geometry.

It was difficult to obtain good films, and this generally gave a low device resistance, low open circuit voltage, V_{oc}, and low short circuit current, I_{sc}, values. Sublimation of a layer of C_{60} on top of a spin-coated film of compound **12** (PPVs donor) led to some improvements of the photovoltaic performance of the device based on **12** (Table 6).

The best results were obtained employing a geometry ITO/PEDOT:PSS/**13**/Al with an output power of 0.86 μW/cm^2 and a fill factor of 25.8%. This could perhaps

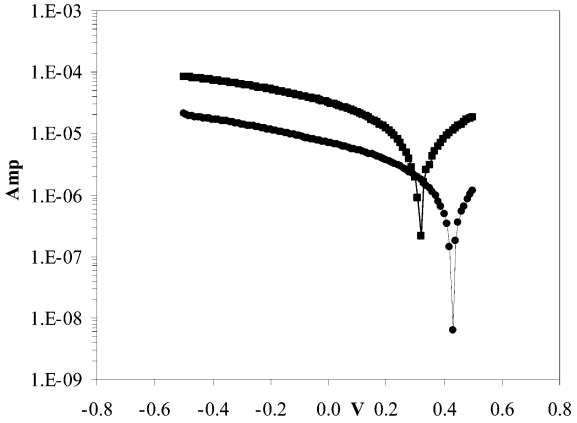

Figure 10. *I/V* comparison between the devices ITO/PEDOT:PSS/**13**/Al (■) and ITO/PEDOT:PSS/**13:18**/Al (●).

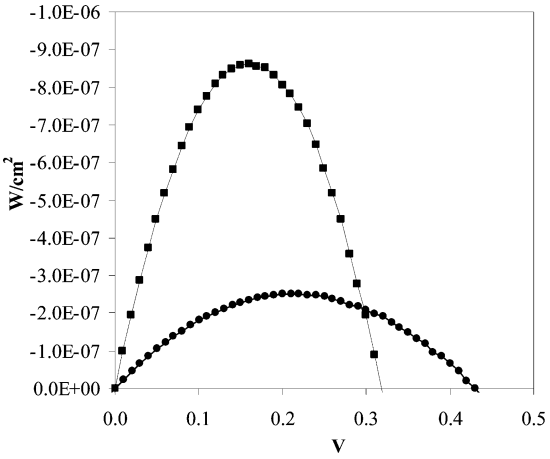

Figure 11. *W/V* comparison between the devices ITO/PEDOT:PSS/**13**/Al (■) and ITO/PEDOT:PSS/**13:18**/Al (●). Despite the higher V_{oc} the cell employing the blend gave a lower power output.

be expected since the ruthenium dye could benefit from the effect of polymer energy transfer as supported by the emission spectroscopy studies showing that the CNOF−tpy emission quantum yield was reduced by 5 times in **13**. Insight into intramolecular energy and electron-transfer processes can guide the realization of optimized blends to produce a solar cell with increased efficiency. Sauvage and co-workers[4b] demonstrated that electron transfer can occur between Zn−porphyrin and Ru complexes, leading to a charge-separated state with a long lifetime that falls under the Marcus inverted region.[25] However, despite the photophysical evidence of partial energy transfer from Zn−porphyrins to ruthenium complexes, the device with ITO/PEDOT:PSS/**13:18**/Al geometry gave lower performance than the device employing **13** alone, producing an output power of 0.25 μW/cm^2 with a fill factor of 25% (Figures 10 and 11). The wavelength dependence of the photovoltaic response was characterized for the three best devices presenting the following geometry: (i) ITO/PEDOT:PSS/**13**/Al, (ii), ITO/PEDOT:PSS/**18**/Al, and (iii) ITO/PEDOT:PSS/**13:18**/Al (see Supporting Information Figures S6 for **18** and Figure S7 for **13:18**).

The wavelength dependence of the ITO/PEDOT:PSS/**13**/Al photovoltaic response is shown in Figure 12, where the presence of a broad peak with a λ_{max} at 400 nm indicates the CNOF−tpy contribution to the charge injection. The superimposition of **13** absorption spectrum also shows the absence of a contribution to the

Table 7. Photovoltaic Performances of DSSC Samples with an Active Area of 2.5 cm² Employing as Electrolyte 0.03 M LiI, 0.03M I_2 in CH_3CN under Standard Illumination (1000 Wm^{-2}, AM1.5, 25 °C)

dye used	I_{sc} (mA/cm²)	V_{oc} (mV)	P_{max} (mW)	FF (%)	efficiency (%)	R_s (Ω)
12	0.11	375	0.05	45.3	0.02	187
13[a]	0.10	395	0.05	52.1	0.02	190
15	0.12	414	0.06	49.6	0.02	173
b	0.08	285	0.02	43.1	0.01	224

[a] Compound **13** has been synthesized using the fraction 6 of **10** (see Supporting Information). [b] A bare TiO_2 electrode was used as a blank test.

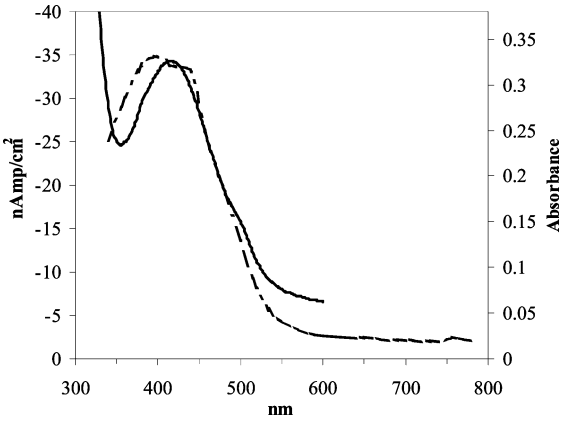

Figure 12. Photocurrent action spectrum (- - -) and absorption spectrum (—) of ITO/PEDOT:PSS/**13**/Al.

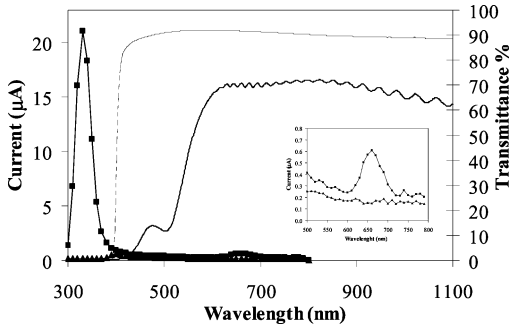

Figure 13. Photocurrent action spectra of **12** with (▲) and without (■) cutoff filter (in the inset zoom of the range between 500 and 800 nm). On the right axis: transmittance spectra of the cutoff filter (- - -) and of **12** absorbed on TiO_2 (—).

photovoltaic response of the MLCT ($d_\pi \rightarrow \pi^*$, Ru → CNOF) absorption band in this experimental condition. The photocurrent action spectrum of the ITO/PEDOT:PSS/**18**/Al devices confirmed a previous observation[23] of an antibatic photovoltaic response to the B (Soret) absorption band while the Q-bands are weakly reflected in the photovoltaic response. The ITO/PEDOT:PSS/**13:18**/Al device configuration which blends **13** and **18** (10 equiv of **18** w/w) showed the charge injection features mostly due to the Zn−porphyrin with two peaks with λ_{max} at 390 and 460 nm antibatic to the B band at 440 nm.

Dye-Sensitized PV Devices. Application of these molecules in dye-sensitized solar cells (DSSCs) has shown better performances than all polymer PV devices, and useful insight into the sensitization of wide-band-gap semiconductors by polymer-based molecules was gained. The realization of DSSCs is reported in the Supporting Information. Absorption on TiO_2 nanocrystalline films was possible even in absence of specific anchoring groups like carboxylate or phosphonate.[26] DSSCs were realized using two different types of liquid electrolytes: 0.03 M LiI, 0.03M I_2 in CH_3CN or 0.25 M $Co(btp)_3ClO_4$, 0.025 M $NOBF_4$ and 0.025 $LiCF_3SO_3$ in methoxypropionitrile. *I/V* and wavelength scans were recorded in the presence and absence of a cutoff filter to discriminate between the TiO_2 direct band-gap sensitization and charge injection from the dyes. Table 7 collects data on the different samples employing the same device geometry (FTO/TiO_2(anat)/TiO_2(nanopor)/dye/electrolyte/Pt/FTO; see Supporting Information). Wavelength scan measurements of DSSCs using iodine-based electrolyte have surprisingly shown no charge injection from the dyes, i.e., no correspondence between absorption spectra and photogenerated current (Figure 13).

Figure 13 indeed shows an intense photocurrent response at 325 nm, an indication that the direct TiO_2 band-gap sensitization was mostly responsible for charge generation. This was furthermore confirmed by a wavelength scan measurement recorded in the presence of a cutoff filter at 390 nm. It can be seen that the presence of the filter suppresses the current induced by direct band-gap excitation as well as the second-order diffraction excitation at 650 nm (inset of Figure 13). The reason for the absence of observable dye charge injection becomes clear from the analysis of the photoanode absorption spectra before the cell assembly and after the cell disassembly. The absorption spectra clearly shows the partial bleaching of the tpy−polymer ligand-centered charge transfer (LCCT) absorption band with $\lambda_{max} \sim 400$ nm, i.e., polymer degradation most probably due to the presence of strong oxidant like the I_2 species (Figure S9 in the Supporting Information).

The use of a different electrolyte such as the $Co(btp)_3ClO_4$[27] allows better cell performances (Table 8) with no dye degradation. The key role of this electrolyte in avoiding polymer degradation is confirmed by the photoaction spectrum which shows clear charge injection from the MLCT (508 nm) and LCCT excitation state of the molecule with a much broader absorption around 380 nm due to the polymer (Figure 14). To confirm the contribution of the dye **12** in current generation, *I/V* characteristics of the device were recorded with (I_{sc} = 0.54 mA/cm², V_{oc} = 255 mV, P_{out} = 0.11 mW) and without (I_{sc} = 0.69 mA/cm², V_{oc} = 265 mV, P_{out} = 0.13 mW)[28] the cutoff filter (Figure S8). A small desorption of the dye after *I/V* measurement was observed. This behavior was expected due to the absence of covalent bonds to the TiO_2 surface (Figure S10).

In conclusion, the application of these new molecules in DSSCs has shown increased performances pointing out the superior results of the molecule **15** which can take effective advantage of the energy transfer processes that occurs in the molecule (see luminescence properties) directing them to an efficient charge injection into the conduction band of the wide-band-gap semiconductors.

Furthermore, it was found of crucial importance the use of a $Co(btp)_3ClO_4$-based electrolyte, which allows

Table 8. Photovoltaic Performances of DSSC Samples with an Active Area of 2.5 cm² Employing 0.25 M $Co(btp)_3ClO_4$, 0.025 M $NOBF_4$, and 0.25 M $LiCF_3SO_3$ in Methoxypropionitrile under Standard Illumination (1000 W m⁻², AM1.5, 25 °C)

dye used	I_{sc} (mA/cm²)	V_{oc} (mV)	P_{max} (mW)	FF (%)	efficiency (%)	R_s (Ω)
12	0.80	315	0.18	29.2	0.07	120
13[a]	0.71	305	0.16	30.1	0.07	107
15	0.71	315	0.22	38.8	0.09	84
b	0.19	235	0.03	28.4	0.01	111

[a] Compound **13** has been synthesized using the fraction 6 of **10** (see Supporting Information). [b] A bare TiO_2 electrode was used as a blank test.

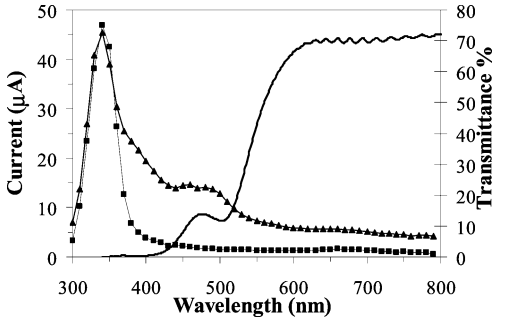

Figure 14. Photocurrent action spectra of bare TiO_2 (■) and dye-sensitized (by **12**) TiO_2 (▲) solar cells. The transmittance spectrum of **12** on TiO_2 is juxtaposed to show the charge injection.

polymer based dye sensitization without the iodine electrolyte drawback of polymer degradation.

Conclusion

We have presented the synthesis of a new monomer and PPV-donor and PPV-acceptor bearing a terminal terpyridine chelating unit. Three new photoactive supramolecular dyads have been prepared by complexing the ruthenium with the PPV−terpyridine ligands. Studies on the incorporation of such ligands and supramolecular building blocks into polymers were performed through photophysical properties. An efficient energy-transfer process from the conjugated polymer block to the metal complex was shown. The best result as organic solar cells was obtained for compound **13**. This result can be due to the longer length of the polymer blocks leading to a more efficient dissociation of the exciton under illumination as well as the electron acceptor character of the CNOF−tpy. Attempts to improve the photoresponse of **13** using a blend of a zinc porphyrin and a ruthenium polymer without a covalent link were not sufficient to improve the photoresponse due to partial intermolecular energy transfer between the ruthenium and the zinc porphyrin. However, improvements can be obtained using an electron acceptor unit such as a fullerene. In the second part of the photovoltaic studies, the coordination polymers were applied in dye-sensitized solar cells, and promising results were obtained with efficiencies ∼0.1%, despite the absence of anchoring groups such as carboxylate. Such a result is very encouraging to develop new terpyridine ligands bearing anchoring groups, and this work is currently in progress. It has also been shown that using $Co(btp)_3ClO_4$ as electrolyte is crucial to avoid polymer degradation obtained with iodine which is commonly used for DSSC's.

Experimental Section

1-Bromo-4-formyl-2,5-dioctylbenzene[10] (**1**), diethyl-4-phosphonatomethylstyrene[11] (**2**), 4-bromo-2,5-dioctyl-4′-vinylstilbene[10] (**3**), vinylacetonitrile[13] (**4**), poly-1,2‴-(2,5-dioctyl-1,4-phenylene-1′,2′-vinylene-1″,4″-phenylene-1‴,2‴-vinylene)[6] (**6**), and 4′-(4-bromophenyl)-2,2′:6′,2″-terpyridine[17] (**8**) were prepared according to the procedures described in the literature. Ruthenium trichloride trihydrate was purchased from Precious Metals Online. Silica gel 60 (0.015−0.040 mm) was employed for the dry column vacuum chromatography. All commercially available reagents were used without further purification. Compounds **9** and **10** were purified using dry column vacuum chromatography according to the procedure reported Pedersen et al.[18]

^1H and ^{13}C NMR spectra were recorded on a 250 MHz Bruker NMR spectrometer at 300 K. UV−vis spectra were taken on a Shimadzu UV-1700 spectrophotometer. Mass spectra (MALDI−TOF) were therefore used as additional proof of the identity of some of the compound. The molecular weight of the polymers was determined by size exclusion chromatography (SEC) using chloroform as eluent and a preparative gel column system consisting of a guard column and two gels columns in succession. The column dimensions were 25 mm diameter × 600 mm, and the pore diameters were 100 and 1000 Å. Polystyrene standards were used for the molecular weight determination. Device preparation is described in detail in the Supporting Information.

Photophysical Methods. All measurements were performed using Spectrosolv grade solvents, and the solutions were degassed for 15 min with argon prior to use. Emission spectra and lifetimes were measured with an instrument comprised of a 450 W Xe lamp for steady-state measurements and a LED for lifetime measurements. The detecting system comprises a single photon counting PMT detector in a peltier cooled housing. All spectra where measured in a perpendicular geometry using a 1 cm quartz cuvettes. Steady-state mesurements where corrected with a 1.8 nm band-pass. The quantum yields were determined using 9,10-diphenylanthracene in cyclohexane[21] as the fluorescence standard. In all cases the optical density was kept below 0.07 to prevent self-absorption. Low-temperature emission spectra were obtained using a cryostat with liquid nitrogen.

Ruthenium(III) 4′-(4-Bromophenyl)-2,2′:6′,2″-terpyridine trichloride was obtained by a method similar to those previously described.[4a,b]

Ruthenium(II) Bis[4′-(4-bromophenyl)-2,2′:6′,2″-terpyridine] $^{2+}$ (16) was prepared according to a procedure published[17b] with the following modifications. A suspension of ruthenium 4′-(4-bromophenyl)-2,2′:6′,2″-terpyridine trichloride (0.20 g, 0.33 mmol) and silver tetrafluoroborate (0.207 g, 1.056 mmol) in acetone (150 mL) was refluxed under argon for 2 h. The precipitate of AgCl formed was removed by filtration through Celite. The filtrate was evaporated to dryness, and the residue was redissolved in absolute ethanol (50 mL) followed by the addition of 4′-(4-bromophenyl)-2,2′:6′,2″-terpyridine (0.13 g, 0.33 mmol), and the solution was heated under reflux and argon overnight. After cooling and evaporation of the solvent, the red residue was dissolved in acetonitrile (50 mL), and a saturated solution of KPF_6 was added. The red precipitate was isolated by centrifugation and purified by chromatography on silica gel with acetonitrile/water/saturated aqueous KNO_3 (14/0.5/1) as eluent. This gave **16** as a red solid in 34% yield (0.098 g).

^1H NMR (250 MHz, $CDCl_3$/DMSO-d_6, 300 K, TMS): $\delta = 8.72$ (s, 4H), 8.35 (d, 4H), 7.59 (d, 4H), 7.26 (s, 4H), 7.14 (s, 4H), 6.69 (d, 4H), 6.53 (t, 4H). MS (MALDI−TOF): *m/z* 876.65, calcd for $C_{42}H_{28}Br_2N_6Ru$ 875.98.

(*E*)-3-(4-Bromo-2,5-dioctylphenyl)-2-(4-vinylphenyl)-acrylonitrile (5). Compound **1**[10] (25 g, 0.061 mol), **4**[13] (8.74 g, 0.061 mol), and sodium methoxide (3.3 g, 0.061 mol) were mixed in a 1 L flask with methanol (300 mL), purged with argon for 10 min, and heated to reflux overnight. The reaction mixture was allowed to cool to room temperature, and water (1 L) was added under stirring. The product was extracted with diethyl ether (3 × 200 mL), and the organic phase was dried over $MgSO_4$, filtered, and evaporated under vacuum to give a clear yellow oil that was recrystallized from absolute ethanol (300 mL) cooled in a bath of acetone/ice dried. This gave **5** as a clear yellow material in 45% yield (14.7 g); mp 39−40 °C. ^{1}H NMR (250.1 MHz, $CDCl_3$, 300 K, TMS): δ = 7.76−7.43 (m, 6H), 6.81−6.69 (m, 1H), 5.84 (d, 1H, J = 18 Hz), 5.35 (d, 1H, J = 11 Hz), 2.68 (dt, 4H, J_1 = 16, J_2 = 7.5 Hz), 1.67−1.54 (m, 4H), 1.37−1.25 (m, 21H), 0.91−0.84 (m, 6H). ^{13}C NMR (62.9 MHz, $CDCl_3$, 300 K, TMS): δ = 141.4, 140.2, 139.6, 138.7, 135.8, 133.5, 131.8, 129.8, 126.8, 126.4, 126.2, 115.3, 113.9, 35.7, 32.9, 31.8, 31.7, 30.9, 29.8, 29.4, 29.3, 29.2, 29.1, 22.6, 22.5, 14.1, 14. Anal. Calcd for $C_{33}H_{44}BrN$: C, 74.14; H, 8.30; N, 2.62. Found: C 74.02; H, 8.58; N, 2.38.

Polymer CNOF 7. A catalytic amount of $Pd_2(dba)_3$ (25 mg) and tri-*tert*-butylphosphine tetrafluoroborate (25 mg) were placed in a 100 mL flask. Anhydrous THF (25 mL) was added, and the mixture was purged with argon for 10 min. *N*-Methyldicyclohexylamine (0.5 mL) was added, and argon purging continued for a few minutes before addition of **5** (0.5 g, 0.935 mmol). The reaction mixture was heated under reflux during 8 h and allowed to cool at room temperature. The solution was poured off in methanol (500 mL) and stirred at room temperature. The precipitated polymer was collected by filtration as an orange solid and purified using a method described in the literature.[14] This gave **7** as an orange solid in 64% yield (0.27 g). ^{1}H NMR (250.1 MHz, $CDCl_3$, 300 K, TMS): δ = 7.87−7.44 (m, 51H), 7.14 (bs, 3H), 7.08 (bs, 2H), 6.86−6.69 (m, 2H), 5.84 (d, 1H), 5.35 (d, 1H), 2.82−2.73 (m, 25H), 1.65 (m, 30H), 1.28 (m, 142 H), 0.88 (bs, 42H). ^{13}C NMR (62.9 MHz, $CDCl_3$, 300 K, TMS): δ = 141.6, 141.5, 141.4, 140.4, 140.3, 140.2, 140.0, 139.9, 138.5, 138.3, 137.4, 135.9, 133.9, 133.5, 132.1, 129.6, 127.4, 126.8, 126.7, 126.4, 126.1, 117.8, 112.6, 32.9, 31.9, 31.8, 31.4, 31.3, 31.2, 31.0, 29.8, 29.6, 29.5, 29.4, 29.3, 29.2, 29.1, 22.6, 14.1. λ_{max} = 417 nm, M_w(SEC) = 6620, M_w/M_n = 1.909.

OF−tpy 9. A catalytic amount of $Pd_2(dba)_3$ (200 mg) and tri-*tert*-butylphosphine tetrafluoroborate (200 mg) were placed in a 250 mL flask. *N*,*N*-Dimethylformamide (100 mL) was added, and the mixture was purged with argon for 10 min. *N*-Methyldicyclohexylamine (2 mL) was added, and argon purging continued for a few minutes before addition of **8** (0.762 g, 1.96 mmol) followed by **3** (2 g, 3.92 mmol). The resulting reaction mixture was heated under reflux for 24 h and then cooled. The solution was poured off in methanol (2 L) and stirred overnight at room temperature. The polymer was collected by filtration as a dark orange solid (2.27 g). The crude polymer was first purified through a silica chromatography column. The first green band was eluted with chloroform, and the second yellow green band was eluted with THF. The solvent was removed from the THF fraction, and 1.89 g of crude polymer was obtained. The polymer was dissolved in a minimum volume of chloroform and purified using a dry column vacuum chromatography.[18] 1,2-Dichloroethane was used as the eluent together with increasing amount of EtOAc in 1% increments. This gave 0.065 g of the fraction 5 of **9** as a yellow viscous solid. ^{1}H NMR (250 MHz, $CDCl_3$, 300 K, TMS): δ = 8.82−8.77 (m, 6H), 7.96 (m, 5H), 7.55−7.03 (m, 48H), 5.81 (bs, 0.8H), 5.23 (bs, 0.9H), 2.76 (m, 19H), 1.64 (m, 15H), 1.29−1.21 (m, 98H), 0.89−0.87 (m, 33H).

This also gave 0.112 g of the fraction 6 of **9** as a yellow viscous solid. ^{1}H NMR (250 MHz, $CDCl_3$, 300 K, TMS): δ = 8.82−8.77 (m, 6H), 7.96 (m, 4H), 7.55−7.02 (m, 40H), 6.68 (d, 0.5H), 5.80 (bs, 0.5H), 5.22 (bs, 0.5H), 2.78−2.69 (m, 13H), 1.64 (m, 9H), 1.29−1.20 (m, 70H), 0.88−0.85 (m, 19H). λ_{max} = 405 nm, M_w(SEC) = 1925, M_w/M_n = 1.182.

CNOF−tpy 10. A catalytic amount of $Pd_2(dba)_3$ (200 mg) and tri-*tert*-butylphosphine tetrafluoroborate (200 mg) were placed in a 250 mL flask. *N*,*N*-Dimethylformamide (100 mL) was added, and the mixture was purged with argon for 10 min. *N*-Methyldicyclohexylamine (2 mL) was added, and argon purging continued for a few minutes before addition of **8** (0.726 g, 1.87 mmol) followed by **5** (2 g, 3.74 mmol). The resulting reaction mixture was heated under reflux during 24 h and then cooled. The solution was poured off in methanol (2 L) and stirred overnight at room temperature. The polymer was collected by filtration as dark orange solid (1.52 g). The crude polymer was first purified through a silica chromatography column. The first green band was eluted with chloroform, and the second orange green band was eluted with THF. The solvent was removed from the THF fraction, and 1.45 g of crude polymer was obtained. The polymer was dissolved in a minimum volume of chloroform and purified using a dry column vacuum chromatography.[18] 1,2-Dichloroethane was used as the eluent together with increasing amount of EtOAc in 1% increments. This gave 0.115 g of the fraction 4 of **10** as an orange viscous solid.

^{1}H NMR (250 MHz, $CDCl_3$, 300 K, TMS): δ = 8.79−8.69 (m, 6H), 7.97−7.15 (m, 66H), 2.82−2.74 (m, 25H), 1.66−1.28 (m, 151H), 0.88−0.85 (bs, 40H). λ_{max} = 405 nm, M_w(SEC) = 7766, M_w/M_n = 2.065.

This also gave 0.175 g of the fraction 5 of **10** as an orange viscous solid. ^{1}H NMR (250 MHz, $CDCl_3$, 300 K, TMS): δ = 8.79−8.69 (m, 6H), 7.92−7.13 (m, 50H), 2.80−2.69 (m, 18H), 1.65−1.27 (m, 113H), 0.87 (bs, 26H). λ_{max} = 405 nm, M_w(SEC) = 4179, M_w/M_n = 1.51.

Preparation of the Ruthenium Polymers. Ruthenium Homopolymer OF−tpy−Ru−tpy−OF 12. To a suspension of $RuCl_3 \cdot 3H_2O$ (0.005 g, 0.019 mmol) in ethanol 99% (7 mL) was added 2 equiv of **9** (0.068 g, 0.038 mmol) in *N*,*N*-dimethylformamide (23 mL), and the suspension was heated 3 h under reflux and argon atmosphere. 3 equiv of silver tetrafluoroborate (0.011 g, 0.057 mmol) was added to the mixture together with acetone (5 mL), and the reflux was continued overnight. The progress of the reaction was followed by MALDI−TOF. The reaction mixture was allowed to cool at room temperature and the silver chloride removed by filtration. The red filtrate was concentrated, and after addition of water, a red precipitate appeared. The precipitate was isolated though centrifugation and washed with water to give 0.070 g of **12**. ^{1}H NMR (250.1 MHz, $CDCl_3$/DMSO-d_6, 300 K, TMS): δ = 9.43 (broad s, 4H), 9.08 (broad s, 4H), 8.44 (broad s, 6H), 7.62−6.95 (m, 147H), 1.54−1.20 (m, 658H), 0.81−0.78 (m, 140H).

Ruthenium Homopolymer CNOF−tpy−Ru−tpy−CNOF 13. To a suspension of $RuCl_3 \cdot 3H_2O$ (0.0054 g, 0.020 mmol) in ethanol 99% (10 mL) was added 2 equiv of **10** (0.097 g, 0.041 mmol) in *N*,*N*-dimethylformamide (23 mL), and the suspension was heated 5 h under reflux and argon atmosphere. 3 equiv of silver tetrafluoroborate (0.011 g, 0.061 mmol) was added to the mixture together with acetone (5 mL), and the reflux was continued overnight. The progress of the reaction was followed by MALDI−TOF. The reaction mixture was allowed to cool at room temperature, and the silver chloride was removed by filtration. The red filtrate was concentrated, and after addition of water a red precipitate appeared. The precipitate was isolated though centrifugation and washed with water to give 0.025 g of **13**. ^{1}H NMR (250.1 MHz, $CDCl_3$, 300 K, TMS): δ = 8.96 (broad s, 4H), 8.68 (d, 4H), 8.28 (broad s, 4H), 8.15 (broad s, 4H), 7.87−7.07 (m, 92H), 3.12 (m, 6H), 2.73 (m, 22H), 1.63−1.27 (m, 198 H), 0.87 (broad s, 26H).

Ruthenium Copolymer OF−tpy−Ru−tpy−CNOF 15. An equimolar solution of **9** (0.065 g, 0.0236 mmol) dissolved in DMF (15 mL) was added to a solution of ruthenium trichloride trihydrate (0.0062 mg, 0.0236 mmol) in ethanol 99% (5 mL), and the suspension was heated under argon at 110 °C overnight. Then 3 equiv of silver tetrafluoroborate (0.014 g, 0.0708 mmol) was added to the reaction mixture together with acetone (10 mL), and the solution was refluxed an additional 2 h. A solution of **10** (0.081 g, 0.0236 mmol) in DMF (15 mL) was added, and the heating continued at 110 °C for 18 h. Then an additional 1 equiv of silver tetrafluoroborate was added (4.6 mg) together with 5 mL of acetone, and the heating of the solution was continued for an additional 24 h. After cooling

and filtration of the silver chloride, the filtrate was concentrated and water was added; a brick orange precipitate appeared. The precipitate was isolated though centrifugation and washed with water to give 0.078 g of **15**. ^{1}H NMR (250.1 MHz, $CDCl_3$/DMSO-d_6, 300 K, TMS): δ = 8.70 (broad s, 4H), 8.33 (broad, 6H), 8.15 (broad s, 2H), 7.93 (broad s, 12H), 7.65 (broad s, 4H), 7.17−6.0 (m, 448H), 2.25−1.17 (m, 114H), 0.81−0.30 (m, 1190H), 0.06 (broad s, 297H).

Acknowledgment. This work was supported by the Danish Technical Research Council (STVF 26-02-0174, STVF 2058-03-0016), the Danish Strategic Research Council (DSF 2104-04-0030) and Public Service Obligation (PSO 103032 FU 3301). We also express sincere gratitude to Ole Hagemann for technical assistance with the SEC measurements and Jan Alstrup for the assistance in the preparation of the cells.

Supporting Information Available: UV−vis spectra of different fractions of CNOF−terpyridine; CNOF−tpy−Ru−tpy−CNOF complexes synthesized from different fractions; standard polymer PV device fabrication and wavelength dependence of the photovoltaic response for the devices **18** and **13**:**18**; dye-sensitized PV devices fabrication; *I/V* characteristics of solar cells sensitized by **12** with and without a cutoff filter at 390 nm; absorption spectra of TiO_2 functionalized by **12** before and after *I/V* characterization with the different electrolytes. This material is available free of charge via the Internet at http://pubs.acs.org.

References and Notes

(1) (a) Ng, P. K.; Gong, X.; Chan, S. H.; Lam, L. S. M.; Chan, W. K. *Chem.−Eur. J.* **2001**, *20*, 4358−4367. (b) El-ghayoury, A.; Schenning, A. P. H. J.; van Hal, P. A.; Weidl, C. H.; van Dongen, J. L. J.; Janssen, R. A. J.; Schubert, U. S.; Meijer, E. W. *Thin Solid Films* **2002**, *97,* 403−404.

(2) (a) Hjelm, J.; Constable, E. C.; Figgemeier, E.; Hagfeldt, A.; Handel, R.;. Housecroft, C. E.; Mukhtar, E.; Schofield, E. *Chem. Commun.* **2002**, 284−285. (b) Hjelm, J.; Handel, R. W.; Hagfeldt, A.; Constable, E. C.; Housecroft, C. E.; Foster, R. J. *J. Phys. Chem. B* **2003**, *107,* 10431−10439. (c) Hjelm, J.; Handel, R. W.; Hagfeldt, A.; Constable, E. C.; Housecroft, C. E.; Foster, R. J. *Electrochem. Commun.* **2004**, *6,* 193−200. (d) Krebs, F. C.; Biancardo, M. *Sol. Energy Mater. Sol. Cells*, in press.

(3) (a) Bignozzi, C. A.; Ferri, V.; Scoponi, M. *Macromol. Chem. Phys.* **2003**, *204*, 1851−1862. (b) Ng, W. Y.; Gong, X.; Chan, W. K. *Chem. Mater.* **1999**, *11*, 1165−1170. (c) Heller, M.; Schubert, U. S. *Macromol. Rapid Commun.* **2002**, *23*, 411−415. (d) Potts, K. T.; Usifer, D. A. *Macromolecules* **1988**, *21*, 1985−1991. (e) Schubert, U. S.; Eschbaumer, C. *Angew. Chem., Int. Ed.* **2002**, *41,* 2892−2926. (f) Hofmeier, H.; Schubert, U. S. *Chem. Soc. Rev.* **2004**, *33*, 373−399. (g) Yu, S. C.; Hou, S.; Chan, W. K. *Macromolecules* **1999**, *32,* 5251−5256.

(4) (a) Collin, J.-P.; Guillerez, S.; Sauvage, J.-P.; Barigelletti, F.; De Cola, L.; Flamigni, L.; Balzani, V. *Inorg. Chem.* **1991**, *30*, 4230−4238. (b) Collin, J.-P.; Harriman, A.; Heitz, V.; Odobel, F.; Sauvage, J.-P. *J. Am. Chem. Soc.* **1994**, *116*, 5679−5690. (c) Flamigni, L.; Barigelletti, F.; Armaroli, N.; Colin, J.-P.; Sauvage, J.-P.; Williams, J. A. G. *Chem.−Eur. J.* **1998**, *4*, 1744. (d) Mikel, C.; Potvin, P. G. *Polyhedron* **2002**, *21*, 49−54. (e) Beley, M.; Bignozzi, C.-A.; Kirsch, G.; Alebbi, M.; Raboin, J.-C. *Inorg. Chim. Acta* **2000**, *318,* 197−200.

(5) (a) Schubert, U. S.; Eschbaumer, C.; Hien, O.; Andres, P. R. *Tetrahedron Lett.* **2001**, *42,* 4705−4707. (b) Schubert, U. S.; Eschbaumer, C.; Nuyken, O.; Hochwimmer, G. *J. Inclusion Phenom. Macrocycl. Chem.* **1999**, *35,* 23−34. (c) Schubert, U. S.; Eschbaumer, C.; Weidl, C. H. *Polym. Mater.: Sci. Eng.* **1999**, *80,* 191−192. (d) Schubert, U. S.; Eschbaumer, C.; Andres, P.; Hofmeier, H.; Weidl, C. H.; Herdtweck, E.; Dulkeith, E.; Morteani, A.; Hecker, N. E.; Feldmann, J. *Synth. Met.* **2001**, *121*, 1249−1252.

(6) Krebs, F. C.; Jørgensen, M. *Macromolecules* **2003**, *36*, 4374−4384.

(7) Krebs, F. C. *Polym. Bull. (Berlin)* **2004**, *52*, 49−56.

(8) (a) Yu, G.; Heeger, A. J. *J. Appl. Phys.* **1995**, *78*, 4510−4515. (b) Granström, M.; Petritsch, K.; Arias, A. C.; Lux, A.; Andersson, M. R.; Friend, R. H. *Nature (London)* **1998**, *395*, 257−260.

(9) Jørgensen, M.; Krebs, F. C. *Polym. Bull. (Berlin)* **2003**, *51*, 23−30.

(10) Krebs, F. C.; Jørgensen, M. *Macromolecules* **2002**, *35*, 10233−10237.

(11) Carbonneau, C.; Frantz, R.; Durand, J.-O.; Lanneau, G. F.; Corriu, R. J. P. *Tetrahedron Lett.* **1999**, *40*, 5855−5858.

(12) Krebs, F. C.; Hagemann, O.; Jørgensen, *M. Sol. Energy Mater. Sol. Cells* **2004**, *83,* 211−228.

(13) Tahan, M. *Isr. J. Chem.* **1972**, *10*, 835−839.

(14) Nielsen, K. T.; Bechgaard, K.; Krebs, F. C. *Macromolecules* **2005**, *38*, 658−659.

(15) Krebs, F. C.; Nyberg, R. B.; Jørgensen, M. *Chem. Mater.* **2004**, *16*, 1313−1318.

(16) Nielsen, K. T.; Spanggaard, H.; Krebs, F. C. *Macromolecules* **2005**, *38*, 1180−1189.

(17) (a) Cave, G. W. V.; Raston, C. L. *J. Chem. Soc., Perkin Trans.* **2001**, *1*, 3258−3264. (b) Kelch, S.; Rehahn, M. *Macromolecules* **1999**, *32*, 5818−5828.

(18) Pedersen, D. S.; Rosenbohm, C. *Synthesis* **2001**, *16*, 2431−2434.

(19) Jørgensen, M.; Krebs, F. C. *J. Org. Chem.* **2004**, *69,* 6688−6696.

(20) (a) De Souza, M. M.; Rumbles, G.; Russell, D. L.; Samuel, I. D. W.; Moratti, S. C.; Holmes, A. B.; Burn, P. L. *Synth. Met.* **2001**, *119*, 635−636. (b) Liu, Y.; Li, Q.; Zhu, D. *Synth. Met.* **2001**, *122*, 401−408. (c) Oelkrug, D.; Tompert, A.; Gierschner, J.; Egelhaaf, H.-J.; Hanack, M.; Hohloch, M.; Steinhuber, E. *J. Phys. Chem. B* **1998**, *102,* 1902−1907. (d) Krebs, F. C.; Jørgensen, M. *Macromolecules* **2002**, *35*, 7200−7206.

(21) Ware, R. W.; Rothman, W. *Chem. Phys. Lett.* **1976**, *39*, 449−453.

(22) *Principles of Fluorescence Spectroscopy*, 2nd ed.; Lakowicz, J. R., Ed.; Kluwer Academic/Plenum Publishers: New York.

(23) Krebs, F. C.; Spanggaard, H. *Sol. Energy Mater. Sol. Cells*, in press.

(24) The absorption peaks of TPH (Zn) are 433, 554, 588, and 626 nm.

(25) Marcus, R. A. *J. Chem. Phys.* **1965**, *43*, 679.

(26) (a) Yang, M.; Thompson, D. W.; Meyer, G. *Inorg. Chem.* **2000**, *39*, 3738. (b) Polo, A. S.; Itokazu, M. K.; Murakami Iha, N. Y. *Coord. Chem. Rev.* **2004**, *248*, 1343−1361.

(27) Sapp, S. A.; Elliott, C. M.; Contado, C.; Caramori, S.; Bignozzi, C. A. *J. Am. Chem. Soc.* **2002**, *124*, 11215−11222.

(28) The data reported in the text for dye **12** are collected from the same photoanode used for the experiment reported in Table 8 and disassembled to record the absorption spectrum in Figure S10. Therefore, the apparent mismatching between Table 8 data and the values reported in the text is a consequence of dye desorption from the TiO_2 film.

MA051274F